The Geological Society of America
Special Paper 483
2011

Theo's Flow, Ontario, Canada: A terrestrial analog for the Martian nakhlite meteorites

R.C.F. Lentz[1,†], T.J. McCoy[2], L.E. Collins[2,3], C.M. Corrigan[2], G.K. Benedix[4], G.J. Taylor[1], and R.P. Harvey[5]
[1]*Hawaii Institute of Geophysics and Planetology, University of Hawaii, Honolulu, Hawaii 96822, USA*
[2]*Department of Mineral Sciences, National Museum of Natural History, Smithsonian Institution, Washington, DC 20560-0119, USA*
[3]*Department of Earth Sciences, University of Southern California, Los Angeles, California 90089-0740, USA*
[4]*Department of Mineralogy, The Natural History Museum, Cromwell Road, London, UK*
[5]*Department of Geology, Case Western Reserve University, Cleveland, Ohio 44106-7216, USA*

ABSTRACT

Martian meteorites provide our only samples for laboratory investigations of Mars, yet the lack of geologic context severely limits their utility. Strong petrologic similarities between the pyroxenitic layer of a 120-m-thick, mafic Archean lava flow in Ontario, Canada, called Theo's Flow, and the nakhlite meteorite group may elucidate geologic processes that operated on Mars. Theo's Flow is in the Abitibi greenstone belt, an area that is well known as a komatiite location. The type locality, and best outcrop, of Theo's Flow is an upturned (~70°) section stretching east-west for ~500 m. Theo's Flow can be divided into distinct lithologic units: a thin basal peridotite (0–9 m), a thick pyroxenite (50–60 m), a gabbro (35–40 m), and a hyaloclastic, brecciated top (8–10 m). It is the thick pyroxenitic layer that bears a striking textural similarity to the Martian nakhlites. Serpentinization of olivine, chloritization of orthopyroxene, and alteration (e.g., pseudomorphic replacement) of plagioclase and minor phases have transformed the original mineral assemblage, though augites remain largely unaltered, and textural relationships are well preserved throughout the flow. Variations in iron and minor-element abundances in augite cores exhibit typical trends for an evolving melt. Bulk rock analyses exhibit elemental trends consistent with an evolving melt, though they exhibit evidence of elemental remobilization by later metamorphism. An average of the peridotite, pyroxenite, and gabbro compositions compares well to that of the quenched top hyaloclastite, suggesting it is a single flow that was differentiated by crystal settling. The lithologic diversity within Theo's Flow suggests that nakhlites may also have complementary lithologies that remain unsampled.

[†]Present address: St. Andrew's Priory School, 224 Queen Emma Square, Honolulu, Hawaii 96813, USA.

Lentz, R.C.F., McCoy, T.J., Collins, L.E., Corrigan, C.M., Benedix, G.K., Taylor, G.J., and Harvey, R.P., 2011, Theo's Flow, Ontario, Canada: A terrestrial analog for the Martian nakhlite meteorites, *in* Garry, W.B., and Bleacher, J.E., eds., Analogs for Planetary Exploration: Geological Society of America Special Paper 483, p. 263–277, doi:10.1130/2011.2483(17).

INTRODUCTION

In spite of more than 30 yr of orbital and in situ observations of Mars, we have yet to return a sample from that planet for study in laboratories on Earth. For this reason, it is fortunate that the solar system has delivered samples of Mars to Earth in the form of meteorites. In the world's collection, there are ~55 distinct meteorites for which overwhelming evidence suggests a Martian origin (McSween and Treiman, 1998). Among these, eight belong to the nakhlite group, which are clinopyroxene (augite) cumulates. Some nakhlites exhibit evidence of extensive preterrestrial aqueous alteration (Treiman, 2005). Like all meteorites, the nakhlites are rocks without geologic context. Orbital data might provide some clues as to the region of origin for these rocks, though we do not know the meter-scale relationships between them or if there remain unsampled lithologies that coexisted with these rocks. This geologic context is essential in order to use these meteorites in understanding the geologic history of Mars.

In Munro Township, eastern Ontario (Fig. 1A), there is an anomalous, differentiated, 120-m-thick lava flow that

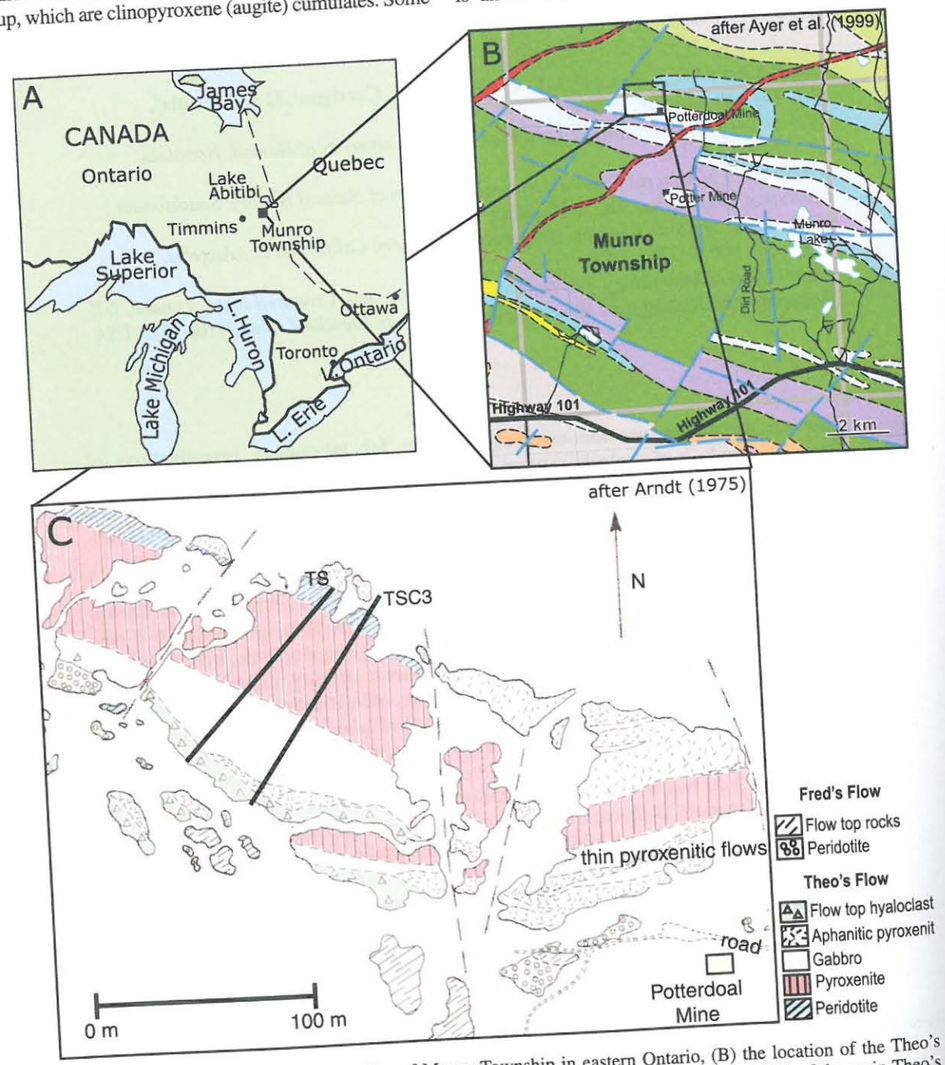

Figure 1. Maps illustrating (A) the location of Munro Township in eastern Ontario, (B) the location of the Theo's Flow area within Munro Township, and (C) the generalized outcrop geology (after Arndt, 1975) of the main Theo's Flow exposure. Traces of our two traverse lines are included for reference. Theo's Flow has an approximate location of 48°37′44″N, 80°13′10″W.

contains peridotite, clinopyroxenite, and gabbro layers capped by a quenched, Al-poor, mafic (MgO ~11 wt%) hyaloclastite. This flow was dubbed Theo's Flow by Arndt (1975, 1977), who first identified and described it. Theo's Flow has taken on new relevance given the recognition of an uncanny resemblance between the clinopyroxenite and the Martian meteorite group known as the nakhlites (Treiman et al., 1995; Lentz et al., 1999).

Lentz et al. (1999) presented a detailed comparison between nakhlites and Theo's Flow. The detailed petrology has also been presented in dissertation form (Friedman, 1998), but the systematic geochemical description of Theo's Flow has never been presented. In this paper, we present results of petrographic and chemical analyses (both mineralogical and whole rock) of Theo's Flow. These descriptions should be particularly useful to the planetary science community as an analog to Mars, owing to the availability of large, representative samples taken systematically through the flow that have been archived for future studies.

GEOLOGIC SETTING

Theo's Flow is in the Archean Abitibi greenstone belt in Canada (Fig. 1A), a region of mafic and ultramafic volcanic units intruded by mafic and felsic plutons and sills (Arndt, 1975). Though the age of Theo's Flow has not been determined, nearby komatiites date from ca. 2.7 Ga (Shirey, 1997), and this is a reasonable approximation for the age of Theo's Flow. Pyroclastics, hyaloclastics, and pillow basalts (Condie, 1981) suggest both subaerial and shallow submarine settings in the area. The belt is extensively folded, producing upturned stratigraphy, and episodic faulting has produced repeated stratigraphic sections on large and small scales. Metamorphic alteration is predominantly greenschist facies, with amphibolite facies limited to areas near felsic plutons.

Theo's Flow lies in the north-central portion of Munro Township (Fig. 1B), an area first mapped by Satterly (1951). It is located north of Highway 101, ~25 km east of the town of Matheson, Ontario. Theo's Flow is reached by driving ~10 km on a series of lightly used logging and mining roads (Fig. 1B). Though no global positioning system (GPS) coordinates were measured at the time of our field work, Theo's Flow has an approximate location of 48°37′44″N, 80°13′10″W. This area is characterized by intrusive and extrusive mafic to ultramafic formations (Arndt, 1975; Johnstone, 1987), including world-famous komatiite exposures (e.g., Arndt et al., 1977; Arndt, 1977, 2008; Fig. 1B). One of these, Fred's Flow, is geographically adjacent to, and stratigraphically above Theo's Flow. Another, Pyke's Hill, is well known for spectacular examples of spinifex-textured komatiite. The type locality, and best outcrop, of Theo's Flow is an upturned (~70°) section stretching east-west for ~500 m (Fig. 1C) that is bounded stratigraphically underneath by an unrelated gabbro, above by the basaltic komatiite Fred's Flow, to the east by a complex of thinner (5–25 m) pyroxenitic flows, and to the west by a fault. The relationships of the east and west boundaries make the orientation of the exposed cross section unclear, although Arndt (1975) reported that regional fabrics and flow features suggest that flow was east to west, implying the outcrop is along-flow.

Metamorphic alteration was chlorite to prehnite-pumpellyite grade (Arndt, 1975; Condie, 1981), causing serpentinization of olivine, chloritization of orthopyroxene, and alteration (e.g., pseudomorphic replacement) of plagioclase and minor phases. Augites are largely unaltered, and textural relationships are well preserved throughout the unit.

SAMPLING AND ANALYTIC METHODS

Three field seasons were spent at Theo's Flow. The first two field seasons included Rachel Lentz (née Friedman), Jeff Taylor, Allan Treiman, and Ralph Harvey. During these field campaigns, smaller samples for petrography were collected along the first line (TS) at ~10 m intervals, with a greater concentration at lithologic boundaries (Fig. 2). Five larger samples (~0.5 kg) were also collected along this line for whole-rock analysis.

The third season (2002) was dedicated to collecting larger samples to be used for further petrologic studies, geochemical studies of representative samples, and archiving of samples for community use. This season included Rachel Lentz, Tim McCoy, Catherine Corrigan, and Gretchen Benedix. The second line (TSC3) was sampled at closer intervals (averaging ~5 m) for a more detailed examination of whole-rock chemistry (Fig. 2). Samples ranging in size from ~1 to 3 kg were collected from each site. A complete set of thin sections and powders for bulk chemical analyses was prepared from each sample. Fresh, unprocessed hand samples remain for future research. These materials are now cataloged as NMNH 117255 in the Rock and Ore collection at the National Museum of Natural History, where they are available for, e.g., petrologic, geochemical, or astrobiological studies. In addition to field sampling, overflights of the field area were made during the third season to provide a broader view of the area (Fig. 3A). To facilitate future visits, aluminum plates were anchored into the rocks with galvanized nails along the second line. In most cases, these were anchored close to sampling sites. In each case, the aluminum tags were stamped with the stratigraphic height at that position, allowing any future visitors to re-mark the same section for additional sampling. As a note to the longevity of these labels, markers from the Arndt field seasons in the 1970s were located and easily deciphered during these field expeditions, ~30 yr later.

For the five large samples collected during the first field season, whole-rock compositions were determined by X-ray fluorescence using a Siemens 303AS X-ray fluorescence spectrometer at the University of Hawaii. For each sample, 300–500 g of material, sufficient to be representative, were cleaned and powdered. Major and minor elements were analyzed in fused glass disks using the methods similar to those of Norrish and Hutton (1969). These analyses are reported to be accurate to better than 1% (Na to within 5%) relative to the measured value. Trace elements were analyzed in pressed powder pellets

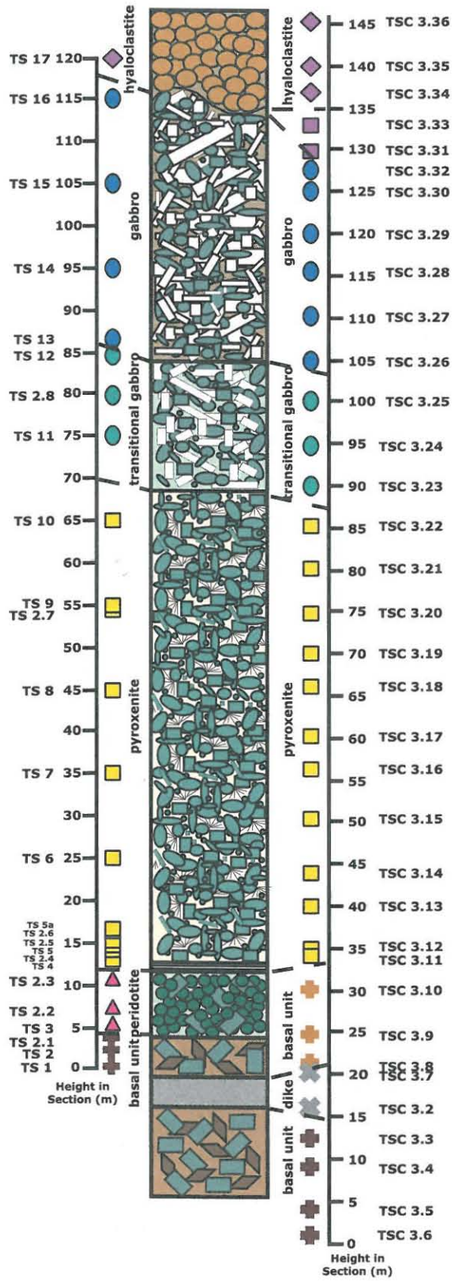

Figure 2. Stratigraphic column of Theo's Flow based on sampling along two traverses. Sample elevations (corrected for bed tilt of 70°) and interpreted lithologic units are illustrated. Note that symbols depicted here are used throughout the following figures to distinguish different lithologic units.

using the technique described by Chappell (1991), and results generally have errors of less than 5% relative.

Quantitative analyses of pyroxenes, amphiboles, and Fe-oxides in thin sections from the first (TS) field season were made on a Cameca SX-50 electron microprobe at the University of Hawaii, using an acceleration voltage of 15 keV, a beam current of 20 nA, and a beam size of 1 μm for 30–90 s (depending on the element). Well-known minerals were used as standards, and all analyses were corrected using a company-supplied ZAF routine (PAP, Pouchou & Pichoir, 1984).

For the systematic geochemical survey (TSC3 samples from the third field season), clean (unweathered) slabs of ~200 g were cut from the initial (~500 g) rough sample. These slabs were further broken into ~1 cm pieces and homogenized. The equipment used for breaking down samples was cleaned with compressed air and alcohol between each sample to prevent contamination. Next, ~25 g samples of the 1 cm pieces were ground into fine powder using aluminum porcelain disks and bowls in an SPEX shatter box, and the resulting powder was sieved to 100 μm. Between each sample, the porcelain disks and bowls were cleaned with washed sea sand until all traces of sample were removed, then washed with Alconox, rinsed with deionized H_2O, and finally rinsed with alcohol. The resulting powders were then prepared separately into fused disks used for bulk major-element analyses, and into pressed pellets for bulk trace-element analyses.

Fused disks (used for major-element analyses) were made by drying ~2.5 g of powdered sample overnight in a 110 °C Thelco oven. A sample of 2.000 g was weighed out using a Metler AE160 balance, placed into a porcelain crucible, and heated in a 1000 °C Lindberg furnace for 2 h. From cooled crucibles, weight was recorded to determine loss on ignition. A sample of 0.4500 g was then mixed with 4.0500 g of lithium tetraborate and shaken with a methylcrylate ball in a SPEX homogenizer for 5 min. This mixture was put into a platinum crucible with 5 drops of lithium iodine and inserted into the Perl 'X3 automatic bead maker.

Pressed pellets were prepared (for trace-element analyses) using an Applied Research Laboratories presser. Aliquots of 2.0 g powdered sample were weighed out and dried in a 110 °C Thelco oven. From that aliquot, 1.6 g of sample and 0.4 g of cellulose were mixed in the shaker. Fused disks were analyzed for major elements, and pressed pellets were analyzed for trace elements, both using a Philips PW1480 automatic sequential wavelength-dispersive X-ray fluorescence spectrometer. Ferrous/ferric iron was determined by wet chemistry with potassium dichromate titration.

RESULTS

Petrography and Field Observations

Theo's Flow can be divided into four distinct lithologic units (Figs. 2 and 3): a thin basal peridotite (0–9 m), a thick pyroxenite (50–60 m), a gabbro (35–40 m), and a hyaloclastic, brecciated top (8–10 m).

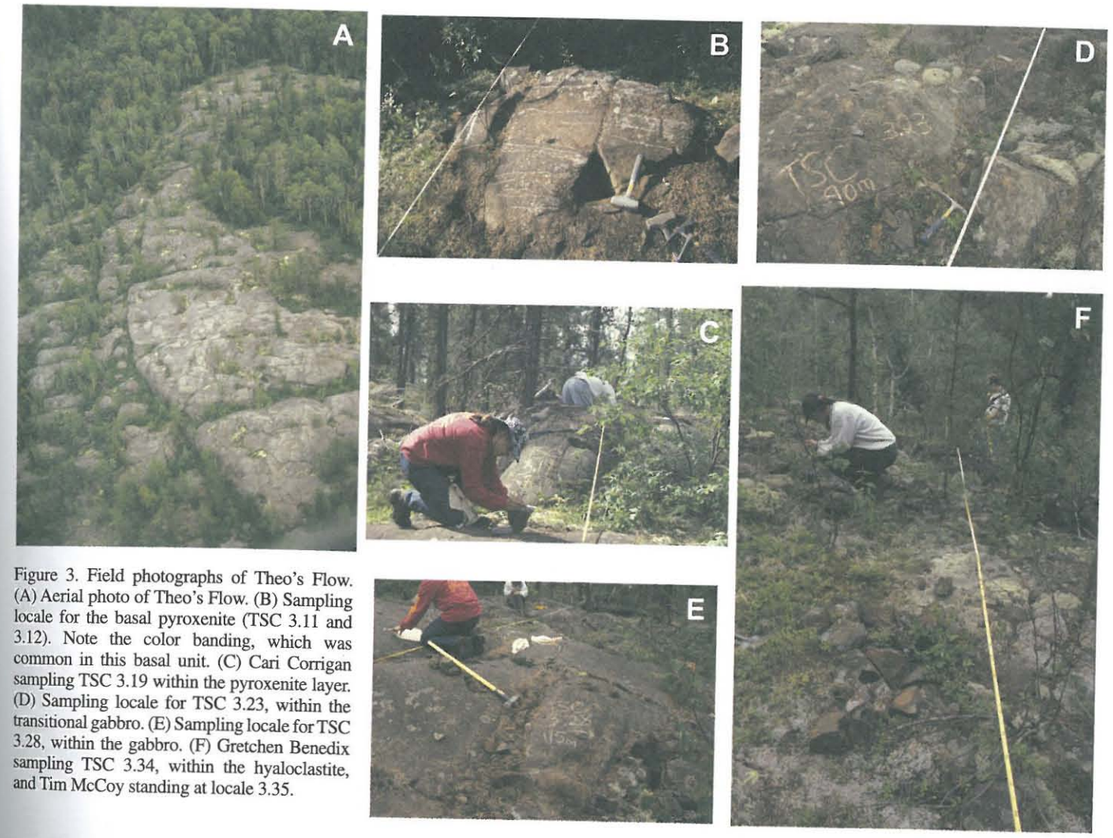

Figure 3. Field photographs of Theo's Flow. (A) Aerial photo of Theo's Flow. (B) Sampling locale for the basal pyroxenite (TSC 3.11 and 3.12). Note the color banding, which was common in this basal unit. (C) Cari Corrigan sampling TSC 3.19 within the pyroxenite layer. (D) Sampling locale for TSC 3.23, within the transitional gabbro. (E) Sampling locale for TSC 3.28, within the gabbro. (F) Gretchen Benedix sampling TSC 3.34, within the hyaloclastite, and Tim McCoy standing at locale 3.35.

Basal Unit

Although Arndt (1977) described an aphanitic pyroxenite and brecciated basal unit for Theo's Flow, mirroring the top of the flow, we could not confirm these lithologies in the field. Instead, we found a basal unit with a faulted lower surface abutting a coarse-grained gabbro. This unit differs from the rest of the flow. It is composed of subequal (~10–20 vol% each) amounts of augite and hornblende. Brown hornblende occurs rimming or partly replacing subhedral augite and as isolated euhedral grains with well-developed 120° cleavage and primary phase morphologies. The euhedral grains commonly display round inclusions, suggesting they are oikocrysts. The inclusions are altered and difficult to identify, but Arndt (1975) speculated that they were serpentinized olivines. These morphologies imply that the hornblende is an original igneous phase, comagmatic with the clinopyroxenes and distinct from other secondary, metamorphic green amphiboles. The presence of these brown amphiboles, along with anomalous compositional trends, suggests that the basal unit is not comagmatic with the rest of Theo's Flow, and it is not discussed further here.

Peridotite (0–9 m Thick)

The true basal unit of Theo's Flow is a serpentinized peridotite. In the field, the basal contact is not obvious, marked only by a subtle change in weathering color. Along our second traverse (TSC3), systematic sampling at 5 m intervals did not find the peridotite, suggesting that it may pinch out locally. The peridotite contains pseudomorphically replaced olivines (equant serpentine outlined by magnetite), large (up to 2 mm wide) poikilitic pyroxenes enclosing replaced olivine (Fig. 4), and minor amounts (1–2 vol%) of spinel with euhedral cores and Ti-rich rims. Brown amphiboles are absent from the peridotite. The abundance of olivine phenocrysts is low (~30 vol%) for a peridotite, although much of the groundmass serpentine and chlorite (55 vol%) may be replaced olivine. Pyroxene in the peridotite grades from orthopyroxene in the lower half (~14 vol%, pseudomorphically chloritized) to clinopyroxene (~10 vol%) in the upper portion of the peridotite.

The transition from peridotite to pyroxenite is characterized by alternating bands of orange (olivine-rich pyroxenite) and dark-gray (olivine-poor pyroxenite) weathering on the

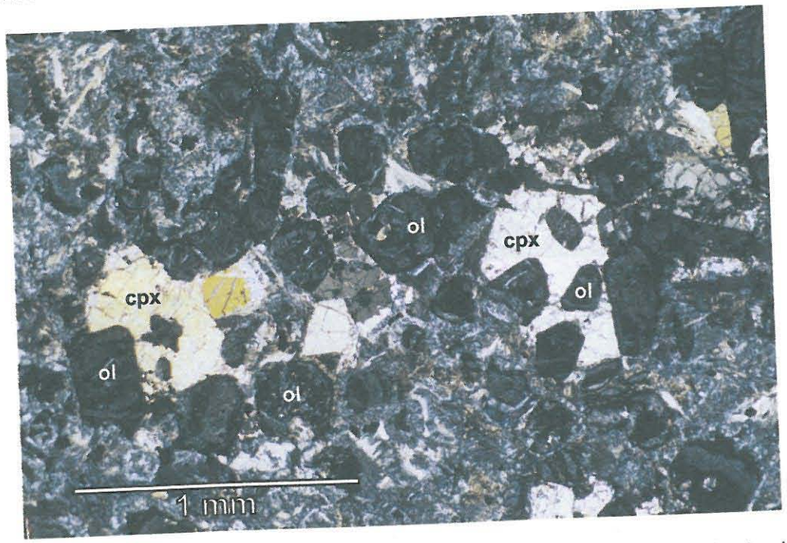

Figure 4. Photomicrograph (crossed nicols) of olivine (ol) phenocrysts almost poikilitically enclosed by Clinopyroxene (cpx) in peridotite. Olivine is serpentinized and rimmed by opaque Fe-oxides.

outcrop (Fig. 3B). Petrographically, the change is marked by a switch from intergrown augite and olivine to smaller augites with interstitial olivine. For several meters above the banded contact, ghostly subhedral pseudomorphs after olivine are present as a minor phase.

Pyroxenite (50–60 m Thick)

The pyroxenite layer is remarkably consistent texturally (Fig. 3C). Clinopyroxene occurs as euhedral to subhedral twinned grains (Figs. 5A and 5B). It is this zone that is texturally similar to the Martian nakhlites (Fig. 5F). Undulatory and bow-tie extinction are not uncommon. Interstitial plagioclase has been largely replaced by prehnite, Epidote, and chlorite, pseudomorphing the plagioclase. The original plagioclase grains are inferred, thus, to be long and thin in habit, arranged in radiating sprays (as is common in nakhlites; Treiman, 2005). There are also sporadic occurrences of spinel and sulfides (pyrite and chalcopyrite).

Augite abundance varies but decreases on average up section (from ~70 to 60 vol%; Fig. 6A; Table 1), whereas plagioclase gradually increases in abundance (from ~10 to 20 vol%). In the pyroxenites, abundances of interstitial groundmass vary widely, and without obvious trend, from 16 to 30 vol%. Sizes of the apparent grain width in >1000 augites per sample were measured in six pyroxenite and two transitional gabbro samples, using digital thin-section images (previously calibrated for scale) and NIH Image software. Within the Theo's Flow pyroxenite, average grain sizes are essentially uniform (on the order of ±50 μm), although maximum grain sizes increase systematically with stratigraphic height (Fig. 6B). The augite grains of the transitional gabbro show a similar average grain size to the pyroxenite. As discussed by Lentz et al. (1999), the pyroxenite also exhibits significant grain clustering, suggesting settling of grains in clumps or chains, rather than as individuals. Plagioclase grain size is also fairly constant throughout the pyroxenite, averaging 50–100 μm in width. Spinel tends to be a fine-grained matrix phase in the pyroxenite, no longer euhedral, and its abundance varies from <1 vol% to nearly 3 vol%.

Gabbro (35–40 m Thick)

The transition from pyroxenite to gabbro is difficult to recognize in the field (Fig. 3D) because the transition is gradual and because plagioclase, the key marker of the gabbro, is

TABLE 1. MODES OF THEO'S FLOW (vol%)

Section	Hgt (m)	Cpyx	Ol	Opx	Amph	Plag	Oxides	Serp	Matrix	Total (%)
TS1	0	20.6			21.6		0.8		57.3	100.3
TS2	1.8	15.2			19.1		2.8	21.2	41.7	100
TS2.1	3.2	9.8			7.6		2.4	22.8	57.3	99.9
TS2.2	6.9	1.3	28.7	14.1			1.9	15.6	38.4	100
TS2.3	10.1	9.3	31.9				1.4	13.6	43.7	99.9
TS4	12.3	62.9	13.6						23.5	100
TS2.4	13.2	50.9	16.6				0.9		31.7	100.1
TS2.5	14.3	68.3	6.7				1.4	6.7	17	100.1
TS2.6	15.4	56	9.9				1.6		32.4	99.9
TS6	23.4	69.9				13.4			16.7	100
TS7	33.1	73.4				9.1			17.5	100
TS8	42.3	58.7				11.1			30.2	100
TS2.7	51.2	60.6				20.3	2.3		16.8	100
TS9	51.7	64.8				16.7			18.5	100
TS10	61.2	60.8				20.9			18.3	100
TS11	70.5	56.8				27			16.2	100
TS2.8	75.1	59.5				27.8	3.4		9.3	100
TS12	79.6	37.7				37.8			24.5	100
TS13	81.5	28.3				51.8			19.9	100
TS14	89.3	26.9				51.6			21.5	100
TS15	98.7	16.7				48.3	6.3		28.7	100
TS17	120		2.05	4.94					93.01	100

Abbreviations: TS—Theo's Section, Hgt—height, (m)—meters, Cpx—clinopyroxene, Ol—olivine, Opx—orthopyroxene, Amph—amphibole, Plag—plagioclase, Serp—serpentine.

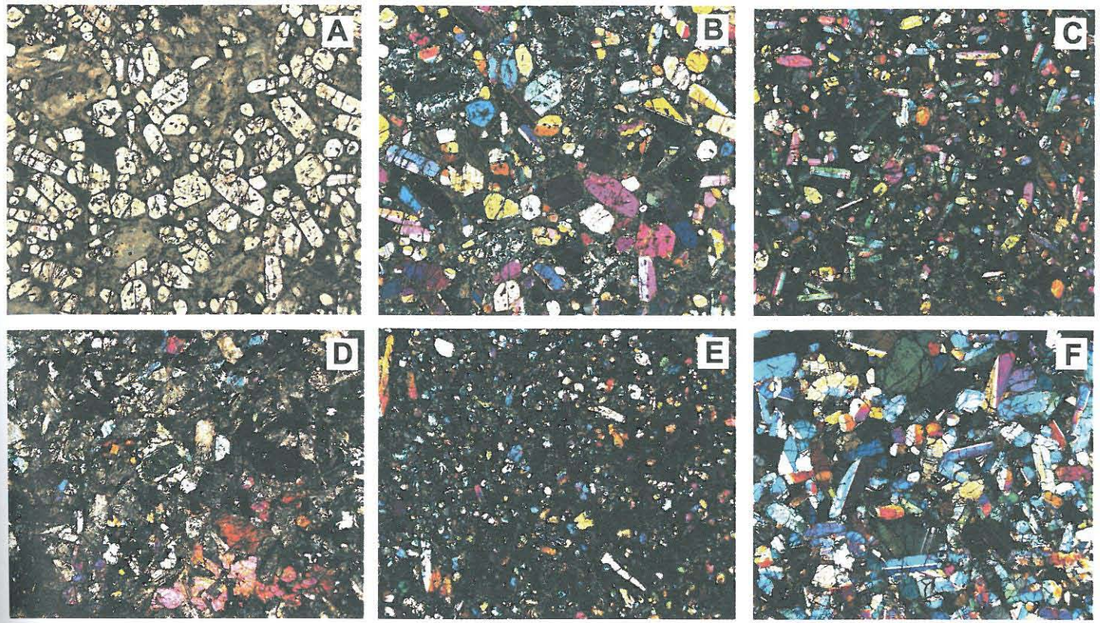

Figure 5. Photomicrographs of (A) TSC 3.12, basal pyroxenite showing euhedral augite with serpentinized olivine (plane-polarized light [PPL]), (B) TSC 3.19, pyroxenite (cross-polarized light [XPL]), (C) TSC 3.23, transitional gabbro (XPL), (D) TSC 3.28, gabbro (XPL), (E) TSC 3.34, hyaloclastite (XPL), and (F) Nakhla, United States National Museum (USNM) 426 (XPL). Field of view in all images is ~6.2 mm.

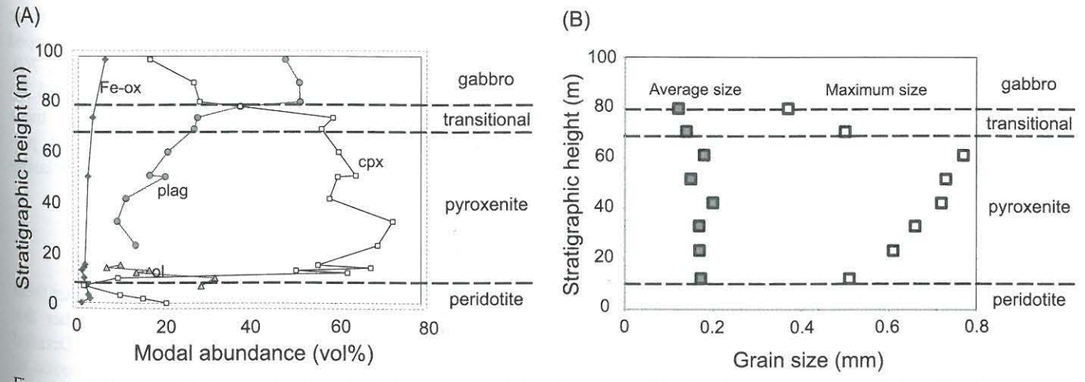

Figure 6. (A) Variation of primary mineral modes with stratigraphic height. Note the shift in abundance of pyroxene and plagioclase (plag) from the pyroxenite into the gabbro. (B) Average (gray symbols) and maximum (open symbols) pyroxene grain sizes throughout the pyroxenite. The greatest change is a drop in the maximum grain size into the transitional gabbro. Iron Oxide (Fe-ox), Olivine (ol) and Clinopyroxene (cpx) are labeled on micrograph.

extensively altered. The lower 15 m of the gabbro, the transitional gabbro, are petrographically distinct from the underlying pyroxenite and overlying gabbro proper. The change from pyroxenite to gabbro is marked by changes in size, shape, and abundance of plagioclase (i.e., its pseudomorphs). At the transition, the average width of plagioclase crystals increases sharply from around 50 μm in the uppermost pyroxenite to >150 μm in the transitional gabbro, which is larger than the cumulus augite grains. Plagioclase in the pyroxenite occurred as sprays of thin tablets, though in the gabbro, plagioclase formed tabular, equant (idiomorphic) grains. Likewise, the abundance of plagioclase increases (Fig. 6A; Table 1) from ~15–20 vol% in

the pyroxenite to 27 vol% in the transitional gabbro. Augite remains euhedral in the transitional gabbro (Fig. 5C), and it is basically indistinguishable from augite in the pyroxenite.

The change from transitional gabbro to true gabbro is also abrupt and marked by a sharp increase in the proportion of plagioclase and then a discontinuous increase to 38 vol%, marking the start of a true gabbro. The gabbro has a typical subophitic texture (Fig. 5D), marked by intergrown euhedra of plagioclase and augite. Moving upward in the section, the abundance of plagioclase increases to 52 vol%, whereas that of augite decreases to 28 vol%. The uppermost portion of the gabbro has an ophitic texture, with plagioclase euhedra partially or completely enclosed by anhedral augite grains.

Minor (<6 vol%) iron oxides occur throughout, with a skeletal cuniform texture. The oxide grains are altered, so original compositions are unknown, but X-ray elemental maps show a correlated abundance of Fe and Ti. In some occurrences, the original titanomagnetite is adorned by a lattice of ilmenite exsolved from the magnetite.

Along our second traverse (TSC3), the uppermost gabbro was capped by a very coarse, nearly pegmatitic, lithology, ~3 m in thickness, that modally is a pyroxenite: 45–55 vol% clinopyroxene, 24–26 vol% plagioclase. This is likely one of several small pegmatitic lenses that Arndt (1975) noted in the area.

Hyaloclastite (8–10 m Thick)

The top layer of the flow is a rubbly, knobby breccia (Fig. 3F). Arndt (1975) described it in detail and called it a hyaloclastite, thereby implying an extrusive, submarine origin for Theo's Flow. The preponderance of altered glass and the fragmental material suggest the material was indeed the product of lava-water interactions, consistent with the theory that much of the region was covered by a shallow sea at the time of Theo's Flow formation (Condie, 1981). Our samples have both altered glass and crystalline fragments (Fig. 5E), sometimes juxtaposed, though the textures gradually become more crystalline with depth. However, even the crystalline areas exhibit quench textures from fine sprays to vermicular and fishbone growths of pyroxene. In the more glassy samples, there are small phenocrysts (0.2–0.3 mm) of pyroxene and serpentinized olivine in minor amounts (~7 vol% total), some displaying skeletal structures with axial cavities.

A feature we did *not* find was a layer beneath the hyaloclastic top of similar bulk composition to the breccia but of medium grain size from more gradual cooling. Such a "roof layer" would be expected to form as heat radiated from the flow's surface if a solidification front were advancing downward (Mangan and Marsh, 1992). Arndt (1975, 1977) mapped an "aphanitic pyroxenite," described as being immediately beneath the hyaloclastite, but of variable thickness. This layer could be the missing roof crust, but we were unable to identify such a lithology in any of our sampling attempts. Our samples show a sharp transition from the pegmatitic pyroxenite to the quenched hyaloclastite.

Mineral Compositions

Pyroxenes in the Pyroxenite and Gabbro

Through most of the pyroxenite and into the gabbro, augites have euhedral cores with thin (<10 μm) Fe-enriched rims. At a given stratigraphic height, augite core compositions are homogeneous but show a gradual, well-defined trend of increasing FeO abundance up section (Fig. 7A; Table 2). Pyroxene rims are more variable. Rim thickness and average composition vary unsystematically with stratigraphic height, although rims do show an overall Fe-enrichment up section, and the difference between core and rim compositions becomes more marked up section.

Variations in minor-element abundances in the cores agree with the Fe trend, exhibiting typical trends for compatible and incompatible elements in an evolving melt (Fig. 7B). Cr_2O_3 displays a typical mafic-compatible decrease up section, whereas Al_2O_3 and TiO_2 (not shown) exhibit mafic-incompatible trends. There is also a subtle leveling off in pyroxene Al_2O_3 concurrent with the increase in plagioclase crystallization at the gabbro.

Pyroxenes in the Hyaloclastic Top and Peridotite

Clinopyroxene core compositions from the peridotite and all but one sample of the hyaloclastite define a trend distinct from that defined by the main flow (Fig. 7C). In incompatible elements like TiO_2 (not shown) and Al_2O_3, the trend is steeper than in the pyroxenite or gabbro, and in Fe#, values span the range covered by the entire pyroxenite. The larger, poikilitic pyroxene of the peridotite is, however, limited to the more magnesian end of the distribution. The smaller grains trapped in the hyaloclastite span the breadth of Fe# range (Fig. 7C). The highest and most glassy sample of hyaloclastite (TSC3.37) contains pyroxene phenocrysts that are significantly more enriched in Fe, and it defines a trend in TiO_2 and Al_2O_3 parallel to that defined by the peridotite and other hyaloclastite samples.

Whole-Rock Compositions

Whole-rock data (Table 3) can help establish whether these units all formed from one parent magma, and whether that magma is truly represented by the hyaloclastic top. Detailed sampling of the flow illustrates a well-defined evolution of composition up section (Fig. 8).

In all elements plotted, the hyaloclastite compositions plot in the middle of the fields described by the pyroxenite and gabbro (Fig. 9). For example, the mafic-incompatible elements (Al, Mn, Y [Fig. 9]; Ti, P, Na, Zr, Nb are not shown) are all depleted with respect to the starting composition (the hyaloclastite) throughout the peridotite and pyroxenite, but they are enriched in the gabbro, where plagioclase has become a liquidus phase (Fig. 9). This reflects a gradual evolution of the melt to more felsic compositions. In contrast, Mg, Ca, and Cr (Fig. 9) are

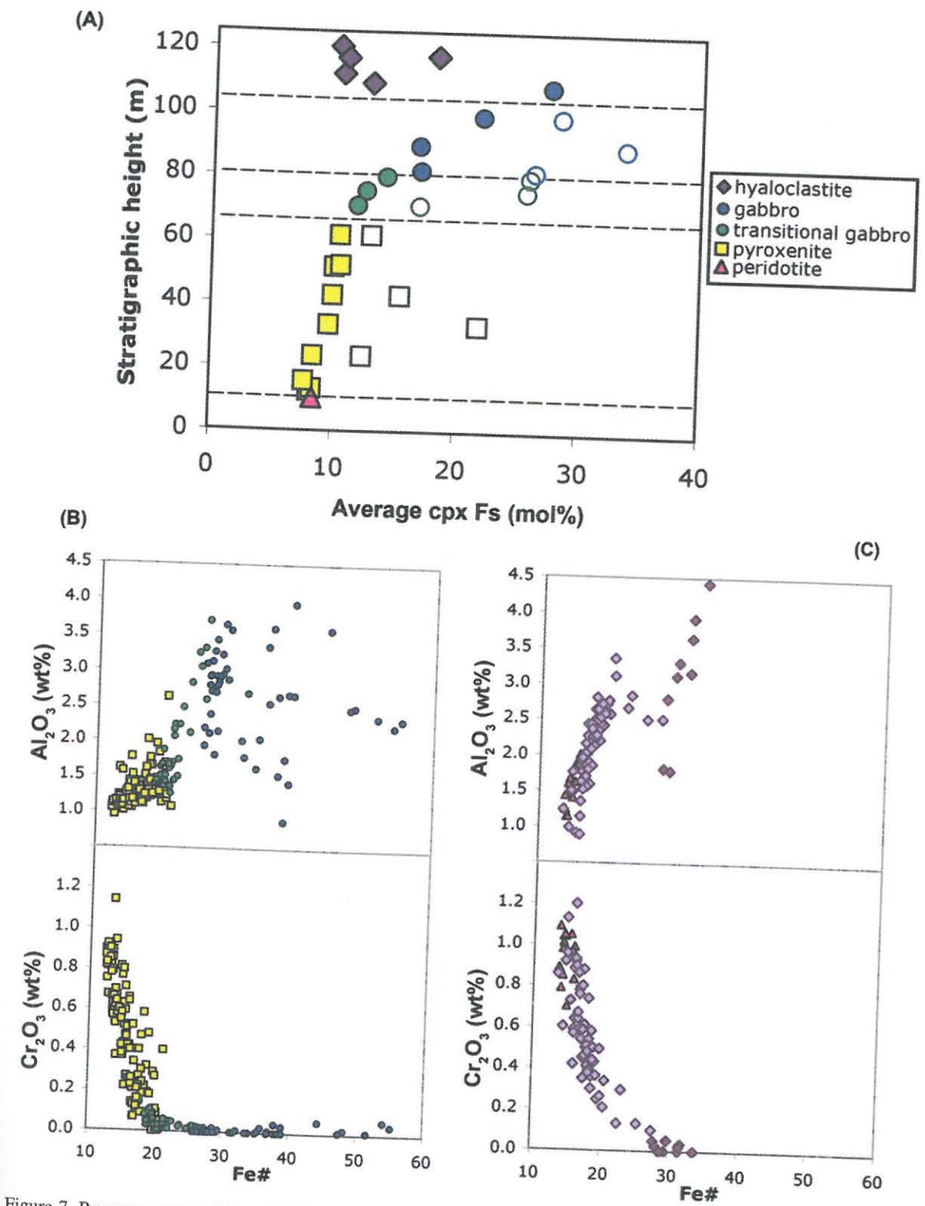

Figure 7. Pyroxene compositions. (A) Average pyroxene Fe enrichment trend in cores (solid symbols) and rims (open symbols) up through the flow. (B) Minor-element trends through pyroxenite, transitional gabbro, and gabbro, illustrating typical incompatible and compatible patterns with magma evolution. (C) Distinctly different trends in pyroxene phenocrysts of the peridotite and hyaloclastite. cpx Fs is ferrosilite (Fs) number from clinopyroxenes (cpx).

TABLE 2. AVERAGE CLINOPYROXENE CORE COMPOSITIONS

Sample:	TS2.3	TS4	TS2.4	TS2.6	TS6	TS7	TS8	TS2.7	TS9	TS10	TS11	TS2.8	TS12	TS13	TS14	TS15	TS16	TSC3.31	TSC3.33	TSC3.34	TSC3.35	TS17	TSC3.36	TSC3.37
Strat. height (m):	10.1	12.3	13.2	15.4	23.4	33.1	42.3	51.2	51.7	61.2	70.5	75.1	79.6	81.5	89.3	98.7	108.1	108.7[†]	111.9	115.9	118.9	120	124.1	124.9
Lithology:	Perid	Pxite	Pxite	Pxite	Pxite	Pxite	Pxite	Pxite	Pxite	Pxite	Trans gab	Trans gab	Trans gab	Gab	Gab	Gab	Gab	Peg pxite	Peg pxite	Hyalo[‡]	Hyalo[‡]	Hyalo[‡]	Hyalo[‡]	Hyalo[‡]
Major oxides (wt%)																								
SiO_2	53.5	53.7	54.0	53.4	53.9	53.6	53.8	53.6	54.0	53.6	52.9	52.9	52.0	51.0	51.7	51.1	49.8	51.7	51.7	51.5	52.6	52.9	51.8	50.2
TiO_2	0.3	0.2	0.2	0.2	0.2	0.3	0.3	0.3	0.3	0.3	0.4	0.4	0.6	0.6	0.6	0.7	1.1	0.5	0.5	0.5	0.3	0.4	0.5	0.7
Al_2O_3	1.6	1.2	1.2	1.2	1.1	1.3	1.5	1.3	1.3	1.3	1.6	1.7	2.8	2.6	2.8	2.3	2.8	2.1	2.3	2.4	1.6	2.2	2.4	3.1
Cr_2O_3	0.9	0.7	0.8	0.8	0.5	0.4	0.3	0.2	0.3	0.1	0.1	0.0	0.0	0.0	0.0	0.0	0.0	0.2	0.2	0.3	0.7	0.6	0.5	0.0
$FeO^{\dagger}$	5.3	5.3	5.4	4.9	5.5	6.2	6.4	6.4	6.8	6.8	7.5	8.0	8.8	10.4	10.5	13.4	16.5	8.5	8.0	8.0	6.6	6.4	6.7	11.1
MnO	0.1	0.2	0.2	0.2	0.2	0.2	0.1	0.2	0.2	0.2	0.2	0.2	0.2	0.2	0.2	0.3	0.5	0.2	0.2	0.2	0.2	0.1	0.2	0.2
MgO	17.4	18.3	18.1	18.0	17.9	17.5	17.5	17.5	17.2	17.6	16.7	16.5	15.8	14.8	15.3	13.2	10.9	16.1	16.4	16.4	17.3	17.3	16.7	14.4
CaO	20.8	20.7	20.4	20.2	21.1	20.7	20.5	20.4	20.7	20.5	20.3	20.3	19.8	19.2	19.1	18.9	18.6	19.8	19.8	19.3	19.9	20.0	20.1	19.1
Na_2O	0.3	0.2	0.2	0.2	0.2	0.2	0.2	0.2		0.2	0.2	0.2	0.3	0.3	0.3	0.3	0.3	0.2	0.2	0.2	0.3	0.3	0.2	0.3
Total	100.3	100.5	100.5	99.1	100.7	100.5	100.7	100.2	100.7	100.6	99.9	100.2	100.2	99.0	100.5	100.1	100.4	99.3	99.4	98.9	99.5	100.3	99.1	99.1
End member calculations for pyroxene minerals																								
Wo	42.3	41.2	41.0	41.1	41.9	41.5	41.1	41.0	41.5	40.7	41.1	41.0	40.7	40.1	39.3	39.6	39.9	40.6	40.5	39.9	40.4	40.7	41.3	40.0
En	49.2	50.6	50.6	51.1	49.6	48.7	48.9	48.9	47.8	48.7	47.0	46.4	45.1	42.9	43.8	38.4	32.6	45.8	46.7	47.2	49.1	49.1	47.8	41.8
Fs	8.5	8.2	8.4	7.8	8.5	9.7	10.0	10.1	10.6	10.5	11.9	12.6	14.2	17.0	16.9	22.0	27.6	13.6	12.7	12.9	10.5	10.2	10.9	18.2
Fe#	14.7	13.9	14.3	13.2	14.6	16.7	17.0	17.1	18.2	17.8	20.2	21.3	23.9	28.4	27.8	36.4	63.6	23.0	21.4	21.3	17.6	17.2	18.5	30.3
No. analyses	17	15	9	11	17	18	9	10	6	19	17	10	9	19	12	9	9	10	10	6	8	41	5	9

Note: Perid—peridotite, Pxite—pyroxenite, Trans gab—transitional gabbro, Gab—gabbro, Peg pxite—pegamatitic pyroxenite, Hyalo—hyaloclastite.
[†]Stratigraphic heights for TSC3 samples were adjusted to TS traverse (by setting base of perodotite/pyroxenite banding to equal height).
[‡]Pyroxene phenocryst compositions within hyaloclastite.

TABLE 3. WHOLE-ROCK X-RAY FLUORESCENCE (ANHYDROUS) COMPOSITIONS

	TS2.2	TS2.3	TSC3.12	TSC3.13	TSC3.14	TSC3.15	TSC2	TSC3.16	TSC3.17	TSC3.18	TSC3.19	TSC3	TSC3.20	TSC3.21	TSC3.22	TSC3.23	TSC3.24	TSC3.25
Strat. height[†] (m):			32.9	37.6	41.3	47.4		53.0	56.7	62.0	65.8		70.4	75.5	80.1	84.6	89.1	94.0
Adjusted height[‡]:	6.9	10.1	13.1	17.8	21.5	27.5	32.4	33.2	36.8	42.2	46.0	51.9	50.6	55.6	60.2	64.7	69.3	74.1
Lithology:	Perid	Perid	Pxite	Pxite	Pxite	Pxite	Pxite	Pxite	Pxite	Pxite	Pxite	Pxite	Pxite	Pxite	Pxite	Trans gab	Trans gab	Trans gab
Major oxides (wt%)																		
SiO_2	44.1	44.5	48.8	51.9	52.8	52.6	52.53	52.4	51.2	52.6	51.7	52.4	52.9	51.8	49.3	51.8	50.4	49.6
TiO_2	0.5	0.5	0.6	0.7	0.7	0.7	0.7	0.7	0.7	0.8	0.7	0.8	0.7	0.8	0.8	1.0	1.0	1.1
Al_2O_3	4.0	3.7	4.7	5.5	5.3	5.1	5.5	5.3	5.3	5.7	5.5	6.1	5.5	6.6	6.4	7.9	8.2	13.2
Fe_2O_3[#]			2.0	2.1	1.5	2.4		1.2	1.8	1.7	1.8		1.4	1.4	2.0	1.3	2.6	2.1
FeO[#]			9.5	7.9	7.7	7.5		8.2	8.6	8.7	8.6		8.8	9.4	11.5	10.7	11.0	11.7
FeO(tot)[#]	14.2	14.3	11.3	9.8	9.0	9.6	10.0	9.3	10.2	10.3	10.3	10.4	10.1	10.6	13.2	11.9	13.3	13.6
MnO	0.2	0.2	0.2	0.2	0.2	0.2	0.2	0.2	0.2	0.2	0.2	0.2	0.2	0.2	0.2	0.2	0.2	0.2
MgO	33.0	30.9	20.1	14.6	14.1	14.4	14.0	14.1	14.4	14.5	14.2	13.2	13.1	12.6	15.1	10.8	11.7	7.1
CaO	2.5	4.3	14.0	16.0	16.3	16.5	15.5	17.0	17.0	15.1	15.9	14.9	15.7	15.4	14.1	13.6	13.4	11.6
Na_2O	0.0	0.0	0.2	1.2	1.5	0.8	0.3	1.1	1.0	0.8	1.2	0.8	1.6	1.9	0.7	2.5	1.7	2.8
K_2O	0.01	0.02	0.0	0.0	0.1	0.0	0.0	0.0	0.0	0.1	0.2	0.0	0.0	0.0	0.1	0.1	0.1	0.6
P_2O_5	0.04	0.03	0.0	0.1	0.1	0.0	0.0	0.0	0.1	0.1	0.1	0.0	0.1	0.1	0.1	0.1	0.1	0.1
Trace elements (ppm)																		
Ni	1336	1181	550	297	271	281	266	264	292	306	270	217	230	199	379	167	266	176
Co	147	138	83	60	57	60	65	56	65	70	65	64	60	62	89	64	81	79
Cr	4071	3135	3122	2673	2213	1745	1316	1379	1402	1367	898	678	650	617	319	350	107	<3<
Rb	1	1	<2<	<2<	2	<2<	<1	<2<	<2<	3	<2<	<1	<2<	<2<	<2<	3	<2<	16
Zn	61	71	99	76	61	100	72	63	73	95	63	65	69	71	90	92	111	92
Cu	25	39	100	119	33	90	71	68	26	119	131	89	86	73	>200>	162	>200>	>200>
V	94	100	199	212	203	210	238	220	229	222	226	258	226	264	238	268	256	241
Sr	5	8	13	33	27	35	117	84	55	50	32	33	27	39	37	61	136	272
Y	7	7	11	14	12	13	15	12	14	15	14	16	14	16	15	20	19	23
Zr	28	24	39	46	42	41	43	41	44	49	45	48	46	50	53	68	69	88
Nb	2	1	3	3	3	3	3	3	3	2	2	3	3	4	4	5	5	7
LOI	9.7	8.9	3.6	1.5	1.2	2.0	2.3	1.9	2.5	1.8	1.6	2.5	1.6	1.5	2.7	1.6	2.3	2.7
Al_2O_3/CaO	1.64	0.88	0.34	0.34	0.32	0.31	0.31	0.31	0.38	0.34	0.35	0.43	0.46	0.58	0.61	1.14	1.36	1.44
Fe#	19.5	20.6	24.0	27.3	26.3	27.3	28.7	27.1	28.4	28.4	29.0	30.6	30.1	32.1	33.0	38.3	38.9	52.0

(*Continued*)

TABLE 3. WHOLE-ROCK X-RAY FLUORESCENCE (ANHYDROUS) COMPOSITIONS (*Continued*)

	TSC4	TSC3.26	TSC3.27	TSC3.28	TSC3.29	TSC3.30	TSC3.32	TSC3.31	TSC3.33	TSC3.34	TSC3.38[§]	TSC3.39[§]	TSC3.35	TSC3.36	TSC3.37	TSCK	Average	Average of lithologies	Difference (wt% or ppm)
Strat. height[†] (m):		98.7	103.6	108.4	112.9	117.6	120.0	122.0	125.0	128.7	128.7	130.6	131.6	136.4	137.2				
Adjusted height[‡]:	82.1	78.8	83.7	88.6	93.0	97.8	100.2	102.1	105.2	108.9	108.9	110.8	111.7	116.6	117.4	120.3			
Lithology:	Gab	Gab	Gab	Gab	Gab	Gab	Gab	Peg pxite	Peg pxite	Hyalo	Hyalo	Hyalo	Hyalo	Hyalo	Hyalo	Hyalo	Hyalo		
Major oxides (wt%)																			
SiO_2	51.5	51.4	51.0	54.2	50.2	50.7	52.2	53.2	51.6	50.5	51.1	54.2	51.0	53.1	50.0	49.74	50.9	51.2	0.2
TiO_2	1.4	1.4	1.2	1.5	1.7	1.8	1.6	1.0	1.1	1.3	1.1	1.1	1.2	1.1	1.1	1.04	1.2	1.0	−0.2
Al_2O_3	14.5	14.6	15.2	13.9	13.8	14.2	14.8	9.6	9.5	10.3	8.9	10.5	10.3	9.1	9.6	8.57	9.4	8.6	−0.8
Fe_2O_3[#]		3.4	1.8	6.7	6.0	4.3	2.2	2.1	2.4	4.6	1.5	1.1	1.9	1.4	2.1				
FeO[#]		10.3	11.3	8.4	10.4	11.8	11.5	8.4	8.5	9.1	11.3	8.6	11.2	9.2	12.1				
FeO(tot)[#]	13.7	13.3	12.9	14.4	15.8	15.7	13.4	10.3	10.7	13.2	13.3	10.5	13.5	12.4	9.7	14.3	12.8	12.0	−0.8
MnO	0.2	0.2	0.2	0.2	0.2	0.2	0.2	0.2	0.2	0.2	0.2	0.1	0.2	0.1	0.2	0.23	0.2	0.2	0.0
MgO	4.9	5.0	5.0	4.0	4.2	5.4	5.1	9.4	9.5	9.8	10.1	10.7	10.4	10.4	11.1	11.92	10.6	11.8	1.2
CaO	9.8	10.7	10.5	7.0	8.9	6.9	7.2	12.9	14.4	11.4	13.0	9.8	10.6	12.2	11.1	11.41	11.6	12.8	1.2
Na_2O	2.2	2.8	3.3	4.2	4.8	4.8	5.1	3.3	2.9	3.1	2.7	3.9	3.2	3.4	2.8	1.11	2.7	2.1	−0.6
K_2O	0.5	0.5	0.6	0.5	0.3	0.2	0.3	0.1	0.0	0.1	0.1	0.1	0.1	0.1	0.0	0.05	0.1	0.2	0.09
P_2O_5	0.1	0.1	0.1	0.2	0.1	0.1	0.2	0.1	0.1	0.1	0.1	0.1	0.1	0.1	0.1	0.07	0.1	0.1	−0.01
Trace elements (ppm)																			
Ni	46	59	71	21	45	42	47	157	158	136	258	119	144	142	534	173	231.2	253.3	22.1
Co	59	56	59	52	65	73	61	54	53	66	73	49	65	56	94	72	71.0	68.5	−2.5
Cr	5	<3<	<3<	<3<	34	<3<	<3<	240	483	266	823	224	288	470	1645	602	682.4	932.3	249.9
Rb	13	11	15	19	10	6	11	<2<	<2<	2	2	2	<2<	<2<	2	<1	1.8	5.4	3.6
Zn	119	132	124	106	146	108	88	62	48	78	114	48	74	48	260	152	120.9	89.9	−31.0
Cu	204	165	156	32	55	84	55	41	31	108	200	121	123	75	157	134	132.7	101.0	−31.7
V	254	226	219	156	257	293	244	239	245	277	234	207	248	247	249	247	250.2	225.2	−25.0
Sr	270	291	313	376	200	274	260	75	60	147	85	98	135	108	42	74	98.5	121.9	23.4
Y	26	24	23	36	29	29	29	18	19	22	20	20	21	21	21	20	20.8	18.5	−2.3
Zr	101	107	101	183	133	133	134	69	73	88	76	80	89	78	81	70	80.3	73.1	−7.2
Nb	6	7	8	14	11	10	10	4	6	7	6	5	7	6	6	4	6.1	5.3	−0.7
LOI	2.1	2.1	2.2	2.0	2.4	2.3	2.6	1.9	1.7	2.3	2.4	1.8	1.8	1.4	2.5	1.5	1.99	2.4	0.4
Al_2O_3/CaO	1.99	1.55	2.05	2.06	0.74	0.66	0.90	0.68	1.08	0.97	0.74	0.86	190.44	0.81	0.67	−0.69	0.82	0.83	0.01
Fe#	61.1	59.9	59.2	67.0	68.1	62.1	59.5	38.2	38.7	43.0	42.5	35.5	42.1	40.2	33.0	40.3	40.3	39.9	−0.4

Note: Perid—peridotite, Pxite—pyroxenite, Trans gab—transitional gabbro, Gab—gabbro, Peg pxite—pegamatitic pyroxenite, Hyalo—hyaloclastite.
[†]Measured stratigraphic heights for TSC, adjusted for bed tilt (70°).
[‡]Stratigraphic heights for TSC traverse adjusted to scale of TS traverse by setting base of peridotite/pyroxenite banding at equal heights (12.3 m).
[§]Stratigraphic heights for TSC3.38 and 3.39 were approximated since the samples were from an outcrop of hyaloclastite off the TSC traverse.
[#]TSC samples had FeO measured by titration. FeO(tot) is all Fe recalculated as Fe^{2+}.

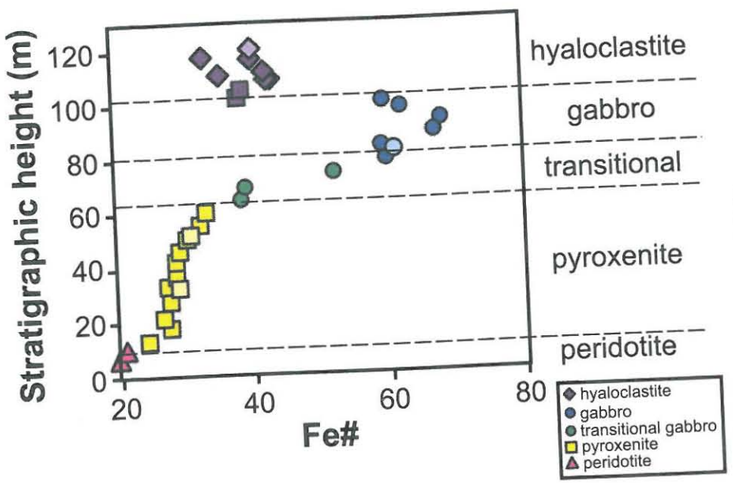

Figure 8. Whole-rock chemistry illustrating the same Fe-enrichment trend with increasing stratigraphic height. Note that the hyaloclastite samples cluster well at intermediate Fe# values.

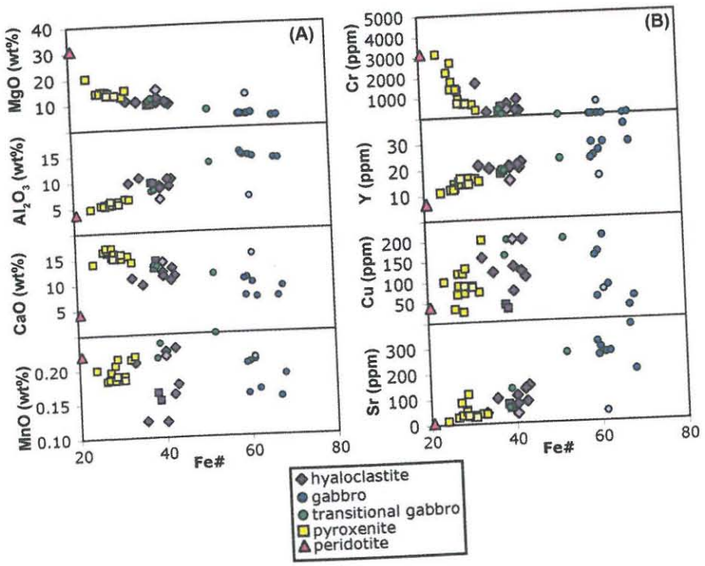

Figure 9. Whole-rock (A) major-, minor-, and (B) trace-element compositions throughout Theo's Flow. Note that most elements display well-defined fractional crystallization trends, with the hyaloclastite samples always falling midway in composition (between the pyroxenite and gabbro). Mn, Sr, and Cu are included to illustrate that a few elements have been affected by later metamorphism and show significant scatter.

enriched relative to the hyaloclastite, consistent with their compatible behavior in mafic systems. Some elements (e.g., Mn, Sr, Cu, Zn) show significant scatter, mostly attributable to processes that occurred during later metamorphism. For example, Cu and Zn were clearly affected by sulfide mobilization that ranged in scale from hand sample to regional.

Theo's Flow has been classified as an Fe-rich tholeiite (Arndt, 1977). Bulk classifications from this study (Table 4), however[S1], suggest that although Theo's Flow is subalkaline and fits within the broad classification of a tholeiite (Arndt, 1977), it is not simply an Fe-rich end member of that class, but instead it is distinct in being noticeably Mg-rich and Al-poor, likely reflecting augite accumulation not observed in other members of this class. The chemical composition of Theo's Flow is even distinct from that of the "average tholeiite" in the Munro area of the Abitibi greenstone belt (Arndt, 1977; Treiman et al., 1996), again by having significantly lower Al_2O_3 and higher FeO and MgO values (Table 4). A factor of particular significance is the

low Al_2O_3/CaO ratio of Theo's Flow, which is consistent with its abundance of augite, and which is similar (among Earth magmas) only to Al-depleted komatiites.

DISCUSSION

We first wanted to establish whether the stratigraphy displayed by Theo's Flow was attributable to a single, differentiated magmatic unit or if it was formed from multiple pulses of melt. In the latter scenario, magma pulses of distinct composition could have generated the different lithologies of Theo's Flow, where each injection would have caused subsequent inflation of the overlying quenched crust. Several lines of evidence argue against multiple magma pulses. First, we might expect distinct boundaries between these units. No such boundaries were observed, either in the field or during detailed petrologic examination of hand samples, although it is possible that such boundaries might be obscured if successive magma pulses were injected quickly relative to the cooling and solidification times. Second, progressive compositional changes in mineral and whole-rock chemistry are more consistent with a single magma. Finally, several units of Theo's Flow (e.g., pyroxenite, peridotite) require unreasonably high liquidus temperatures. Theo's Flow more likely represents a single magmatic pulse.

To test the idea that these units are comagmatic and represent differentiation of a single starting composition, we averaged peridotite, pyroxenite, and gabbro compositions taken at 5 m intervals across the flow (Table 3). We compared this composition to an average of the hyaloclastite, which is thought to represent an upper quenched margin. These two compositions exhibit a remarkably good match (<20% variation) in most major, minor, and trace elements (Table 3; Fig. 10). Exceptions include the water-soluble elements Na, K, and Rb and the chalcophiles Cu, Zn, and Cr, all of which were likely redistributed during regional greenschist metamorphism. The compositional similarity among these units supports the hypothesis that the quenched breccia top is representative of the originally erupted magma composition and that all of the lithologies are derived from one parent magma. Theo's Flow apparently samples a single, differentiated magma unit, though it probably did not erupt as one 120-m-thick body of lava, but instead ponded in an area constrained by local topography.

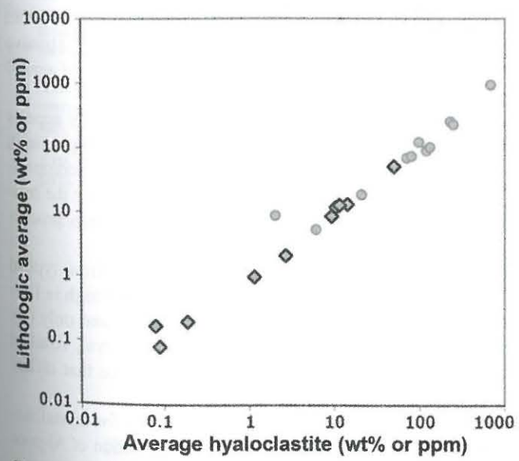

Figure 10. Comparison of average measured hyaloclastic breccia composition and calculated bulk composition, found by averaging all lithology compositions throughout the flow (Table 3). Good agreement of nearly all elements (majors, minors [diamonds], and traces [circles]) suggests that the hyaloclastic top represents the original magma composition from which the other lithologies formed. Deviations likely represent more mobile elements affected by later metamorphism (e.g., Rb, K).

Archean volcanism in much of the Abitibi greenstone belt is thought to have taken place in a shallow-marine setting (Condie, 1981). The upper layer of Theo's Flow lava was thus exposed to water upon eruption. As it quenched, it reacted explosively, forming meters of rubbly breccia during and after emplacement. Much of the breccia probably remained loosely consolidated, like "a'a lava clinker," with no continuous glassy cap to prevent seawater from circulating freely. The permeability of the upper breccia and the circulation of seawater would have made for a higher heat flux, and a faster cooling rate at the surface than if the flow had erupted subaerially (Keszthelyi, 1995). The lower portions of the breccia, however, may have been warm enough for the broken pieces to be partly welded back together into a more solid surface that was coherent and buoyant enough not to sink into the underlying molten lava, instead acting to partly insulate the flow's interior.

Based on the composition of the hyaloclastite, the insulated pool of lava was initially quite hot compared to typical basaltic magmas. The liquidus temperature of the bulk composition was calculated using liquid-solid equilibrium models (e.g., melts [http://melts.ofm-research.org/#RefGS]; Ghiorso and Sack, 1995) to be ~1240 °C. The high temperature and highly mafic composition mean that the melt had a low viscosity of ~8 Pa-s (MELTS; Ghiorso and Sack, 1995), which is much lower than the typical basaltic viscosity of 100–1000 Pa-s (Francis, 1993).

In a normal basaltic system, like a lava lake, material crystallizing in the upper reaches of the melt pool tends to be trapped as the solidification front progresses down from the upper surface, forming a roof crust (Marsh, 1988, 1989; Mangan and Marsh, 1992). Amalgamations of co-crystallized pyroxene and plagioclase grains are less dense than the underlying melt and, therefore, fail to sink quickly enough to escape the advancing front. The viscosity of the basaltic melt is also high enough to inhibit settling (Mangan and Marsh, 1992).

In Theo's Flow, the conditions were different. The quenched breccia trapped some phenocrysts, but only small ones. With progressive cooling through the rubbly breccia, the topmost layer of melt cooled sufficiently in a few days to begin nucleation and growth. In this zone, augite began crystallizing under steady-state conditions of nucleation and growth. Since the parent magma composition was so Al-poor, augite remained the sole liquidus phase for a long temperature interval. Further, the

melt was more than an order of magnitude less viscous than a typical basaltic melt, allowing olivine and pyroxene phenocrysts to sink.

Although our findings are consistent with progressive crystallization and settling to form the related units within Theo's Flow, the mechanism by which this layering formed remains elusive. Since the growing pyroxene grains were denser than the average underlying melt (3.2 g/cm^3 vs. 2.7 g/cm^3), they may have initially sunk in a manner efficient enough that no crustal material built up beneath the hyaloclastite. As crystallization continued, settling of individual crystals would have been inhibited, but fragments of cumulate rock (glomerocrysts) might have settled as complete units (Marsh, 2002), where grain growth could have occurred either in the upper crystallization zone or in the growing cumulate pile at the bottom, with only nucleation and minimal growth at the top (Mangan and Marsh, 1992). This makes it difficult to account for the near uniformity in grain size and pyroxene core compositions noted throughout the 60-m-thick pyroxenite layer. Alternatively, vigorously convecting magma in the "lava lake" could have swept up pyroxene-rich glomerocrysts into circulating cells, with pyroxene grains protected from resorption within the melt/crystal cluster (and they possibly could even have continued to grow). Once the parcels of crystal/melt suspension settled out of the main melt pool, they added to the growing cumulus pile. Each cluster probably flattened slightly upon impact, squeezing out some interstitial fluid and contributing to the modal concentration of grains. The remaining interstitial melt then evolved more rapidly, encouraging the growth of Fe-enriched pyroxene rims and the addition of interstitial plagioclase.

An important outcome of this work is that it becomes difficult to imagine a mechanism by which the Martian nakhlite pyroxenites, so similar in so many aspects (texture, mineralogy, and geochemistry) to Theo's pyroxenite, could be produced without accompanying lithologies formed through a similar melt evolution. By analogy, nakhlites may not represent the only, or even the dominant, lithology within their parental lava flows. Instead, clinopyroxenites like the nakhlites likely have associated peridotites, gabbros, and quench-textured rocks. These latter lithologies might be expected to comprise up to 50% of the parental lava flow. A search for nakhlite source regions (Hamilton et al., 2003) focused on signatures of the clinopyroxene-rich, nakhlite-like spectral end member. Hamilton et al. (2003) did not find extensive areas with compositions consistent with the nakhlites, though they were limited to identifying lithologies exposed only at the uppermost surface. The pyroxenite at Theo's Flow is observable because the stratigraphy has been uplifted to expose it. There is little evidence to date for extensive uplift and/or tilting of rocks on Mars, so the result of Hamilton et al. (2003) may not be surprising and should not be taken to indicate that such lithologies might not be common on Mars. They may only be exposed intact in, for example, canyon and/or crater walls. Additionally, nakhlite lava flows might indeed be rich in clinopyroxene, though the upper reaches of such flows might be expected to be gabbroic or similar in bulk composition to the hyaloclastite. The impact process might excavate basal olivine or clinopyroxene cumulates, but these lithologies would be intimately mixed at the scale of most orbital remote-sensing footprints. Thus, caution must be exercised in search for nakhlite source regions or craters.

Despite these difficulties, a search for the nakhlite source region(s) is of particular importance for comparative planetology. The close association of Theo's Flow and komatiitic flows within the Abitibi greenstone belt might suggest that the nakhlite source region also occurs with associated komatiitic lavas. If this true, it offers an extraordinary opportunity to understand a process for which the record has been erased on Earth. Although Archean komatiites are well known on Earth, no modern exposures of their volcanic edifices have been preserved (Arndt, 2008). Arndt (2008) argued that komatiitic volcanoes were likely to have been broad, low shields, built of geochemically related flows and shallow intrusions. Further, lava flows emanating from such volcanoes likely change from proximal, channelized flows to distal, sheet-like flows. A planetary example would be Hadley Rille at the *Apollo 15* site on the Moon, and its thin flows in Mare Imbrium. While evidence of these edifices has been erased by nearly 3 b.y. of geologic activity on Earth, the relatively young nakhlites (ca. 1.3 Ga) suggest that such edifices could be preserved on Mars, providing a snapshot of a geological process that may have operated widely on terrestrial planets in their earlier history.

CONCLUSIONS

This study suggests several interesting conclusions about the formation of Theo's Flow, in particular, and thick extrusive flows in general:

(1) The lithologic diversity present within Theo's Flow appears to have resulted from differentiation in a single magma unit, rather than through multiple injections of distinct composition. The bulk composition is best represented by the hyaloclastite. The exact nature of the differentiation process remains uncertain.
(2) The bulk composition of Theo's Flow differs from typical tholeiitic melts, being markedly poor in Al and high in Fe + Mg. This composition, with its low viscosity and only one liquidus phase over a long temperature interval, resulted in crystallization and a solidification sequence that differs markedly from other basaltic magma bodies.
(3) Theo's Flow may provide the best analog yet for crystallization of some magmas on Mars. The combination of Al-poor compositions and thick lava flows (favored by the lower gravity of Mars compared to Earth) may have produced the Martian clinopyroxenite parent magma body that was sampled as nakhlite meteorites. The lithologic diversity present within Theo's Flow suggests that complementary peridotites and gabbros might also exist in the same terrain on Mars.

ACKNOWLEDGMENTS

We would like to thank Allan Treiman for early inspiration and perspiration in the field. We would also like to thank Allan Treiman and Vicky Hamilton for insightful and useful reviews that made this a better paper. We thank Nicole Lunning for her efforts in revising figures and reviewing text edits. Funding for this work was supplied by the National Science Foundation Graduate Research Fellowship, National Aeronautics and Space Administration (NASA) grants NAG 54212 (K. Keil) and NAGW 3684 (G. Jeffrey Taylor), and the Becker Endowment to the Smithsonian Institution.

REFERENCES CITED

Arndt, N.T., 1975, Ultramafic Rocks of Munro Township and their Volcanic Setting [Ph.D. dissertation]: Toronto, University of Toronto, 295 p.
Arndt, N.T., 1977, Thick, layered peridotite-gabbro lava flows in Munro Township, Ontario: Canadian Journal of Earth Sciences, v. 14, p. 2620–2637, doi:10.1139/e77-227.
Arndt, N.T., 2008, Komatiite: New York, Cambridge University Press, 467 p.
Arndt, N.T., Naldrett, A.J., and Pyke, D.R., 1977, Komatiitic and iron-rich tholeiitic lavas of Munro Township, northeast Ontario: Journal of Petrology, v. 18, p. 319–369.
Ayers, J.A., Berger, B.R., and Trowell, F., 1999, Geological Compilation of the Lake Abitibi Greenstone Belt: Ontario Geological Survey Map 3398, scale 1:100,000.
Basaltic Volcanism Study Project (BVSP), 1981, Basaltic Volcanism on the Terrestrial Planets: New York, Pergamon Press, 1286 p.
Chappell, B.W., 1991, Trace element analysis of rocks by X-ray spectrometry: Advances in X-Ray Analysis, v. 34, p. 263–276.
Condie, K.C., 1981, Archean greenstone belts, *in* Condie K.C., ed., Developments in Precambrian Geology: Amsterdam, Netherlands, Elsevier, 434 p.
Francis, P., 1993, Volcanoes: A Planetary Perspective: Oxford, Oxford University Press, 521 p.
Friedman, R.C., 1998, Petrologic Clues to Lava Flow Emplacement and Post-Emplacement Processes [Ph.D. dissertation]: Honolulu, University of Hawaii at Manoa, 260 p.
Ghiorso, M.S., and Sack, R.O., 1995, Chemical mass transfer in magmatic processes: IV. A revised and internally consistent thermodynamic model for interpolation and extrapolation: Contributions to Mineralogy and Petrology, v. 119, p. 197–212, doi:10.1007/BF00307281.
Hamilton, V.E., Christensen, P.R., McSween, H.Y., Jr., and Bandfield, J.L., 2003, Searching for the source regions of Martian meteorites using MGS TES: Integrating Martian meteorites into the global distribution of igneous materials on Mars: Meteoritics & Planetary Science, v. 38, p. 871–885, doi:10.1111/j.1945-5100.2003.tb00284.x.
Johnstone, R.M., 1987, Geology of the Stoughton-Roquemaure Group, Beatty and Munro Townships, Northwestern Ontario [M.S. thesis]: Ottawa, Carleton University, 325 p.
Keszthelyi, L., 1995, A preliminary thermal budget for lava tubes on the Earth and planets: Journal of Geophysical Research, v. 100, p. 20,411–20,420, doi:10.1029/95JB01965.
Lentz, R.C.F., Taylor, G.J., and Treiman, A.H., 1999, Formation of a Martian pyroxenite: A comparative study of the nakhlite meteorites and Theo's Flow: Meteoritics & Planetary Science, v. 34, p. 919–932, doi:10.1111/j.1945-5100.1999.tb01410.x.
Mangan, M.T., and Marsh, B.D., 1992, Solidification front fractionation in phenocryst-free sheet-like magma bodies: The Journal of Geology, v. 100, p. 605–620, doi:10.1086/629611.
Marsh, B.D., 1988, Crystal capture, sorting, and retention in convecting magma: Geological Society of America Bulletin, v. 100, p. 1720–1737, doi:10.1130/0016-7606(1988)100<1720:CCSARI>2.3.CO;2.
Marsh, B.D., 1989, Magma chambers: Annual Review of Earth and Planetary Sciences, v. 17, p. 439–472, doi:10.1146/annurev.ea.17.050189.002255.
Marsh, B.D., 2002, On bimodal differentiation by solidification front instability in basaltic magmas: Part 1. Basic mechanics: Geochimica et Cosmochimica Acta, v. 66, p. 2211–2229, doi:10.1016/S0016-7037(02)00905-5.
McSween, H.Y., Jr., and Treiman, A.H., 1998, Martian meteorites, *in* Papike, J.J., ed., Planetary Materials: Washington, D.C., Mineralogical Society of America, p. 6-1–6-53.
Norrish, K., and Hutton, J.T., 1969, An accurate X-ray spectrographic method for the analysis of a wide range of geologic samples: Geochimica et Cosmochimica Acta, v. 33, p. 431, doi:10.1016/0016-7037(69)90126-4.
Pouchou & Pichoir, 1984, Recherche Aérospatiale, v. 5, p. 349–351.
Satterly, J., 1951, Geology of Munro Township: Ontario Department of Mines Annual Report, v. 60(8), p. 1–60.
Shirey, S.B., 1997, Initial Os isotopic compositions of Munro Township, Ontario, komatiites revisited: Additional evidence for near-chondritic, late-Archean convecting mantle beneath the Superior Province, *in* Abstracts of the 7th Goldschmidt Conference: LPI Contribution 921, Abstract 2375.
Treiman, A.H., 2005, The nakhlite meteorites: Augite-rich igneous rocks from Mars: Chemie der Erde, v. 65, p. 203–270, doi:10.1016/j.chemer.2005.01.004.
Treiman, A.H., Taylor, G.J., and Friedman, R.C., 1995, Nakhla and its lookalikes: Al-depleted magmas and mantle differentiation on Mars and the Earth: Houston, Texas, Lunar and Planetary Institute, Lunar and Planetary Science Conference XXVI, p. 1419–1420.
Treiman, A.H., Norman, M., Mittlefehldt, D., and Crisp, J., 1996, "Nakhlites" on Earth: Chemistry of clinopyroxenites from Theo's Flow: Ontario, Canada, LPS, v. XXVII, p. 1341–1342.

Manuscript Accepted by the Society 2 February 2011

Printed in the USA